6

THE HODGKIN–HUXLEY MODEL OF ACTION POTENTIAL GENERATION

The vast majority of nerve cells generate a series of brief voltage pulses in response to vigorous input. These pulses, also referred to as *action potentials* or *spikes*, originate at or close to the cell body, and propagate down the axon at constant velocity and amplitude. Fig. 6.1 shows the shape of the action potential from a number of different neuronal and nonneuronal preparations. Action potentials come in a variety of shapes; common to all is the all-or-none depolarization of the membrane beyond 0. That is, if the voltage fails to exceed a particular threshold value, no spike is initiated and the potential returns to its baseline level. If the voltage threshold is exceeded, the membrane executes a stereotyped voltage trajectory that reflects membrane properties and not the input. As evident in Fig. 6.1, the shape of the action potential can vary enormously from cell type to cell type.

When inserting an electrode into a brain, the small all-or-none electrical events one observes extracellularly are usually due to spikes that are initiated close to the cell body and that propagate along the axons. When measuring the electrical potential across the membrane, these spikes peak between +10 and +30 mV and are over (depending on the temperature) within 1 or 2 msec. Other all-or-none events, such as the complex spikes in cerebellar Purkinje cells (Fig. 6.1G) or bursting pyramidal cells in cortex (Fig. 6.1H and Fig. 16.1C), show a more complex wave form with one or more fast spikes superimposed onto an underlying, much slower depolarization. Finally, under certain conditions, the dendritic membrane can also generate all-or-none events (Fig. 6.1H) that are much slower than somatic spikes, usually on the order to 50–100 msec or longer. We will treat these events and their possible significance in Chap. 19.

Only a small fraction of all neurons is unable—under physiological conditions—to generate action potentials, making exclusive use of graded signals. Examples of such *nonspiking cells*, usually spatially compact, can be found in the distal retina (e.g., bipolar, horizontal, and certain types of amacrine cells) and many neurons in the sensory-motor pathway of invertebrates (Roberts and Bush, 1981). They appear to be absent from cortex,

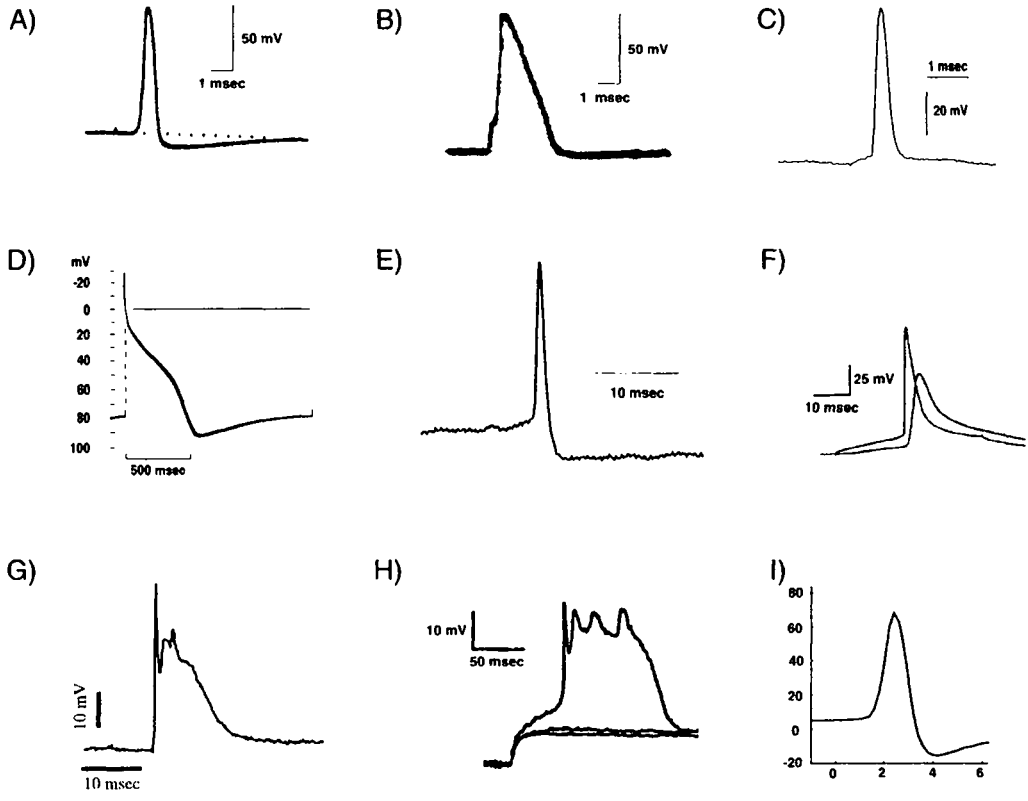

Fig. 6.1 Action Potentials of the World Action potentials in different invertebrate and vertebrate preparations. Common to all is a threshold below which no impulse is initiated, and a stereotypical shape that depends only on intrinsic membrane properties and not on the type or the duration of the input. **(A)** Giant squid axon at 16° C. Reprinted by permission from Baker, Hodgkin, and Shaw (1962). **(B)** Axonal spike from the node of Ranvier in a myelinated frog fiber at 22° C. Reprinted by permission from Dodge (1963). **(C)** Cat visual cortex at 37° C. Unpublished data from J. Allison, printed with permission. **(D)** Sheep heart Purkinje fiber at 10° C. Reprinted by permission from Weidmann (1956). **(E)** Patch-clamp recording from a rabbit retinal ganglion cell at 37° C. Unpublished data from F. Amthor, printed with permission. **(F)** Layer 5 pyramidal cell in the rat at room temperatures. Simultaneous recordings from the soma and the apical trunk. Reprinted by permission from Stuart and Sakmann (1994). **(G)** A complex spike—consisting of a large EPSP superimposed onto a slow dendritic calcium spike and several fast somatic sodium spikes—from a Purkinje cell body in the rat cerebellum at 36° C. Unpublished data from D. Jaeger, printed with permission. **(H)** Layer 5 pyramidal cell in the rat at room temperature. Three dendritic voltage traces in response to three current steps of different amplitudes reveal the all-or-none character of this slow event. Notice the fast superimposed spikes. Reprinted by permission from Kim and Connors (1993). **(I)** Cell body of a projection neuron in the antennal lobe in the locust at 23° C. Unpublished data from G. Laurent, printed with permission.

thalamus, cerebellum, and associated structures (although it is difficult, on *a priori* grounds, to completely rule out their existence).

Action potentials are such a dominant feature of the nervous system that for a considerable amount of time it was widely held—and still is in parts of the theoretical community— that all neuronal computations only involve these all-or-none events. This belief provided much of the impetus behind the neural network models that originated in the late 1930s and early 1940s (Rashevsky, 1938; McCullough and Pitts, 1943).

The ionic mechanisms underlying the initiation and propagation of action potentials in nervous tissue were elucidated in the squid giant axon by a number of workers, most notably by Hodgkin and Huxley in Cambridge, England (1952a,b,c,d). Together with Eccles, they shared the 1963 Nobel prize in physiology and medicine. (For a historical account see Hodgkin, 1976.) Their quantitative model (Hodgkin and Huxley, 1952d) represents one of the high points of cellular biophysics and has been extremely influential in terms of enabling a large class of quite diverse membrane phenomena to be analyzed and modeled in terms of simple underlying variables. This is all the more surprising since the kinetic description of membrane permeability changes within the framework of the Hodgkin–Huxely model was achieved without any knowledge of the underlying ionic channels.

A large number of excellent papers and books describing in great detail various aspects of the Hodgkin–Huxley model are available today. Nothing matches the monograph by Jack, Noble, and Tsien (1975) for its 200-page extended coverage of various analytical and numerical approaches to understand all relevant aspects of initiation and conduction of action potentials. Cronin (1987) presents a mathematical account of the more formal aspects of Hodgkin and Huxley's model as well as related models, while Scott (1975) pays particular attention to questions of interest to physicists and applied mathematicians. The books by Hille (1992), Johnston and Wu (1995) and Weiss (1996) provide up-to-date and very readable accounts of the biophysical mechanisms underlying action potentials in neuronal tissues. The edited volume by Waxman, Kocsis, and Stys (1995) concentrates on the morphology and the pathophysiology of myelinated and unmyelinated axons.

Because the biophysical mechanisms underlying action potential generation in the cell body and axons of both invertebrates and vertebrates can be understood and modeled by the formalism Hodgkin and Huxley introduced 40 years ago, it becomes imperative to understand their model and its underlying assumptions. We will strive in this chapter to give an account of those properties of the Hodgkin–Huxley model that are of greatest relevance to understanding the initiation of the action potential. We will also discuss the propagation of spikes along unmyelinated and myelinated fibers. Chapter 9 extends the Hodgkin–Huxley framework to the plethora of other currents described since their days.

6.1 Basic Assumptions

Hodgkin and Huxley carried out their analysis in the giant axon of the squid. With its half-millimeter diameter, this fiber is a leviathan among axons. (The typical axon in cortex has a diameter more than 1000 times smaller; Braitenberg and Schüz, 1991.) In order to eliminate the complexity introduced by the distributed nature of the cable, a highly conductive axial wire was inserted inside the wire. This so-called *space clamp* keeps the potential along the entire axon spatially uniform, similar to the situation occurring in a patch of membrane. This, together with voltage clamping the membrane and the usage of pharmacological agents to block various currents, enabled Hodgkin and Huxley to dissect the membrane current into its constitutive components. The total membrane current is the sum of the ionic currents and the capacitive current,

$$I_m(t) = I_{\text{ionic}}(t) + C_m \frac{dV(t)}{dt} . \tag{6.1}$$

With the help of these tools, Hodgkin and Huxley (1952a,b,c) carried out a large number of experiments, which lead them to postulate the following *phenomenological* model of the

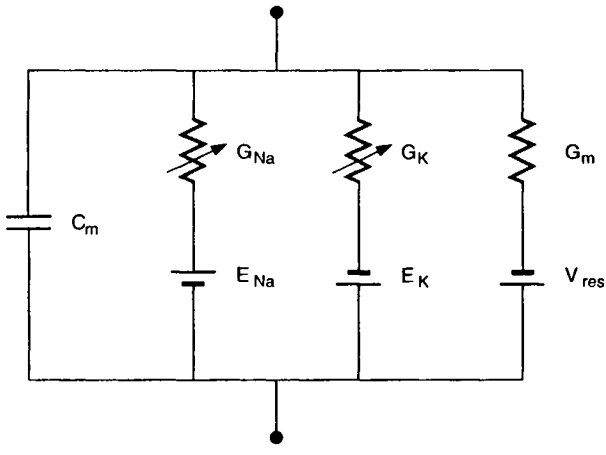

Fig. 6.2 Electrical Circuit for a Patch of Squid Axon Hodgkin and Huxley modeled the membrane of the squid axon using four parallel branches: two passive ones (membrane capacitance C_m and the leak conductance $G_m = 1/R_m$) and two time- and voltage-dependent ones representing the sodium and potassium conductances.

events underlying the generation of the action potential in the squid giant axon (Fig. 6.2; Hodgkin and Huxley, 1952d).

1. The action potential involves two major voltage-dependent ionic conductances, a sodium conductance G_{Na} and a potassium conductance G_K. They are independent from each other. A third, smaller so-called "leak" conductance (which we term G_m) does not depend on the membrane potential. The total ionic current flowing is the sum of a sodium current, a potassium current, and the leak current:

$$I_{ionic} = I_{Na} + I_K + I_{leak} . \tag{6.2}$$

2. The individual ionic currents $I_i(t)$ are linearly related to the driving potential via Ohm's law,

$$I_i(t) = G_i(V(t), t)(V(t) - E_i) \tag{6.3}$$

where the ionic reversal potential E_i is given by Nernst's equation for the appropriate ionic species. Depending on the balance between the concentration difference of the ions and the electrical field across the membrane separating the intracellular cytoplasm from the extracellular milieu, each ionic species has such an associated *ionic battery* (see Eq. 4.3). Conceptually, we can use the equivalent circuit shown in Fig. 6.2 to describe the axonal membrane.

3. Each of the two ionic conductances is expressed as a maximum conductance, $\overline{G}_{Na}$ and $\overline{G}_K$, multiplied by a numerical coefficient representing the fraction of the maximum conductance actually open. These numbers are functions of one or more fictive *gating particles* Hodgkin and Huxley introduced to describe the dynamics of the conductances. In their original model, they talked about *activating* and *inactivating* gating particles. Each gating particle can be in one of two possible states, open or close, depending on time and on the membrane potential. In order for the conductance to open, all of these gating particles must be open simultaneously. The entire kinetic properties of their model are contained in these variables. We will consider the physical and molecular interpretation of these gating particles in terms of numerous all-or-none microscopic *ionic channels* in Chap. 8.

6.2 Activation and Inactivation States

Let us specify how these activation and inactivation states determine the two ionic currents. This is important, since the vast majority of state-of-the-art ionic models is formulated in terms of such particles.

6.2.1 Potassium Current I_K

Hodgkin and Huxley (1952d) model the potassium current as

$$I_K = \overline{G}_K n^4 (V - E_K) \tag{6.4}$$

where the maximal conductance $\overline{G}_K = 36$ mS/cm^2 and the potassium battery is $E_K = -12$ mV relative to the resting potential of the axon. n describes the state of a fictional *activation particle* and is a dimensionless number between 0 and 1. Note that with today's physiological conventions, I_K as outward current is always positive (for $V \geq E_K$; see Fig. 6.5).

Chapter 8 treats the underlying microscopic and stochastic nature associated with the macroscopic and deterministic current. Let us for now develop our intuition by assuming that the probability of finding one activation particle in its *permissive* or open state is n (and it will be with probability $1 - n$ in its *nonpermissive* or closed state where no current flows through the conductance). Equation 6.4 states that in order for the channel to be open, the four gating particles must simultaneously be in their open state. We can also think of n as the proportion of particles in their *permissive* state; potassium current can only flow if four particles are in their permissive state.

If we assume that only these two states exist (for a single particle) and that the transition from one to the other is governed by first-order kinetics, we can write the following reaction scheme:

$$n \underset{\alpha_n}{\overset{\beta_n}{\rightleftharpoons}} 1 - n \tag{6.5}$$

where α_n is a voltage-dependent rate constant (in units of 1/sec), specifying how many transitions occur between the closed and the open states and β_n expresses the number of transitions from the open to the closed states (in units of 1/sec). Mathematically, this scheme corresponds to a first-order differential equation,

$$\frac{dn}{dt} = \alpha_n(V)(1 - n) - \beta_n(V)n\,. \tag{6.6}$$

The key to Hodgkin and Huxley's model—as well as the most demanding part of their investigation—was the quantitative description of the voltage dependency of the rate constants. Instead of using rate constants α_n and β_n, we can reexpress Eq. 6.6 in terms of a voltage-dependent time constant $\tau_n(V)$ and a steady-state value $n_\infty(V)$ with

$$\frac{dn}{dt} = \frac{n_\infty - n}{\tau_n} \tag{6.7}$$

where

$$\tau_n = \frac{1}{\alpha_n + \beta_n} \tag{6.8}$$

and

$$n_\infty = \frac{\alpha_n}{\alpha_n + \beta_n}. \tag{6.9}$$

Both descriptions, either in terms of rate constants α_n and β_n or in terms of a time constant τ_n and a steady-state variable n_∞, are equivalent. While Hodgkin and Huxely used the former, we will use the latter, due to its simpler physical interpretation.

One of the most striking properties of the squid membrane is the steepness of the relation between conductance and membrane potential. Below about 20 mV, the steady-state potassium membrane conductance G_K increases e-fold by varying V by 4.8 mV, while the voltage sensitivity of the sodium conductance is even higher (an e-fold change for every 3.9 mV). For higher levels of depolarization, saturation in the membrane conductance sets in (Hodgkin and Huxley, 1952a). This steep relationship must be reflected in the voltage dependency of the rate constants. Hodgkin and Huxley (1952d) approximated the voltage dependencies of the rate constants by

$$\alpha_n(V) = \frac{10 - V}{100(e^{(10-V)/10} - 1)} \tag{6.10}$$

and

$$\beta_n(V) = 0.125e^{-V/80} \tag{6.11}$$

where V is the membrane potential relative to the axon's resting potential in units of millivolt. Figure 6.3 shows the voltage dependency of the associated time constant and the steady-state value of the potassium activation variable. While τ_n has a bell-shaped dependency, n_∞ is a monotonically increasing function of the membrane potential. The curve relating the steady-state potassium conductance to the membrane potential is an even steeper function, given the fourth-power relationship between G_K and n. This is a hallmark of almost all ionic conductances: depolarizing the membrane potential increases its effective conductance.[1] One of the few exceptions is the appropriately named *anomalous rectifier* current I_{AR} (frequently also termed *inward rectifier*), which turns on with increasing membrane hyperpolarization (Spain, Schwindt, and Crill, 1987).

The fraction of the steady-state potassium conductance open at any particular voltage $\overline{V}$, that is, for $t \to \infty$, is identical to $n_\infty(\overline{V})^4$. At V_{rest} this number is very small, $n_\infty(0)^4 = 0.01$, that is, only about 1% of the total potassium conductance is activated. Using the voltage-clamp setup, we now move the membrane potential as rapidly as possible to $\overline{V}$ and clamp it there. The evolution of the potassium conductance is dictated by the differential Eq. 6.7,

$$n(t)^4 = \left(n_\infty - (n_\infty - n_0)e^{-t/\tau_n(\overline{V})}\right)^4, \tag{6.12}$$

where n_0 is the initial value of the potassium activation, $n_0 = n_\infty(0) = 0.32$, and n_∞ its final value, $n_\infty = n_\infty(\overline{V})$. The time course of any one activation variable follows an exponential, a reflection of the underlying assumption of a first-order kinetic scheme. The time course of the fourth power of $n(t)$ is plotted on the right-hand side of Fig. 6.4, following a sudden shift in the membrane potential, from rest to the various voltage values indicated. Superimposed are the experimentally measured values of the potassium conductance. It is remarkable how well the points fall onto the curve. Upon stepping back to the original membrane potential, n slowly relaxes back to its original low value.

These rate constants have a probabilistic interpretation, covered in more depth in Chap. 8.

1. Whether or not the associated ionic current also increases depends on the relevant ionic reversal potential (Eq. 6.3).

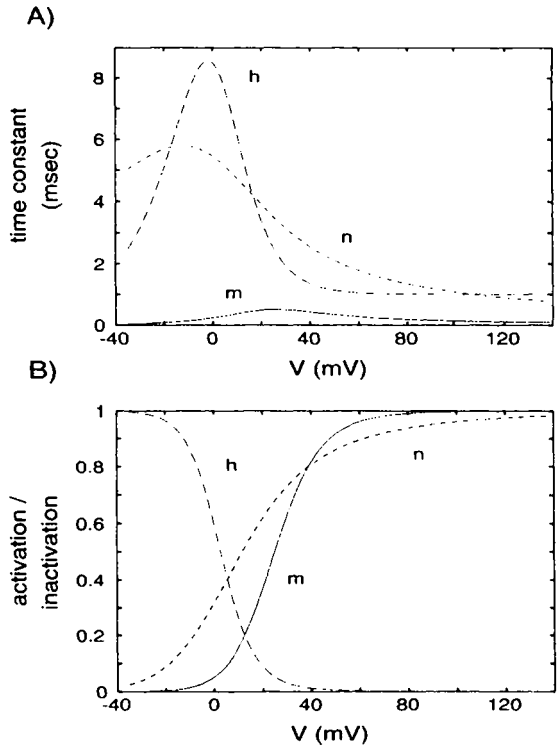

Fig. 6.3 VOLTAGE DEPENDENCY OF THE GATING PARTICLES Time constants **(A)** and steady-state activation and inactivation **(B)** as a function of the relative membrane potential V for sodium activation m (solid line) and inactivation h (long dashed line) and potassium activation n (short, dashed line). The steady-state sodium inactivation h_∞ is a monotonically decreasing function of V, while the activation variables n_∞ and m_∞ increase with the membrane voltage. Activation of the sodium and potassium conductances is a much steeper function of the voltage, due to the power-law relationship between the activation variables and the conductances. Around rest, G_{Na} increases e-fold for every 3.9 mV and G_K for every 4.8 mV. Activating the sodium conductance occurs approximately 10 times faster than inactivating sodium or activating the potassium conductance. The time constants are slowest around the resting potential.

6.2.2 Sodium Current I_{Na}

As can be seen on the left hand side of Fig. 6.4, the dynamics of the sodium conductance that we will explore now are substantially more complex.

In order to fit the kinetic behavior of the sodium current, Hodgkin and Huxley had to postulate the existence of a sodium activation particle m as well as an *inactivation particle* h,

$$I_{Na} = \overline{G}_{Na} m^3 h (V - E_{Na}) \tag{6.13}$$

where $\overline{G}_{Na}$ is the maximal sodium conductance, $\overline{G}_{Na} = 120\,\text{mS/cm}^2$, and E_{Na} is the sodium reversal potential, $E_{Na} = 115$ mV, relative to the axon's resting potential. m and h are dimensionless numbers, with $0 \leq m, h \leq 1$. By convention the sodium current is negative, that is, inward, throughout the physiological voltage range (for $V < E_{Na}$; see Fig. 6.5).

The amplitude of the sodium current is contingent on four hypothetical gating particles making independent first-order transitions between an open and a closed state. Since these

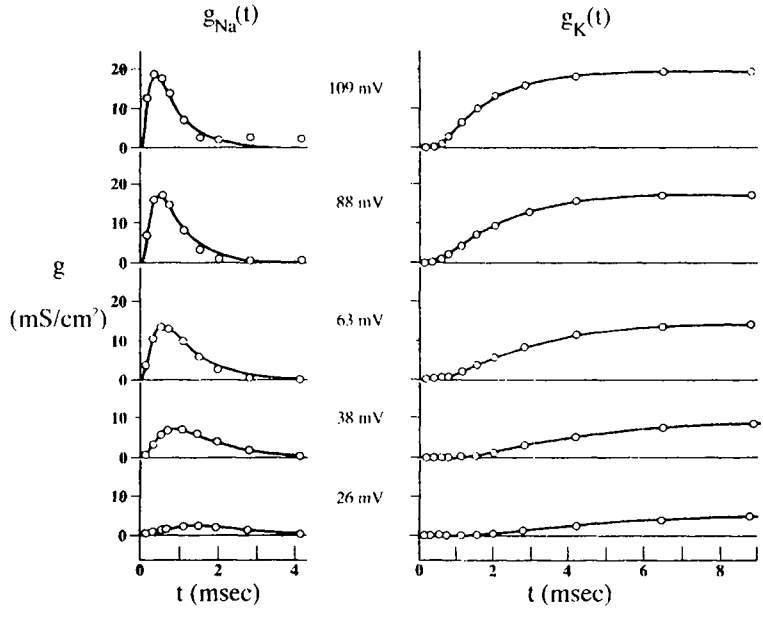

Fig. 6.4 K^+ AND Na^+ CONDUCTANCES DURING A VOLTAGE STEP Experimentally recorded (circles) and theoretically calculated (smooth curves) changes in G_{Na} and G_K in the squid giant axon at 6.3° C during depolarizing voltage steps away from the resting potential (which here, as throughout this chapter, is set to zero). For large voltage changes, G_{Na} briefly increases before it decays back to zero (due to *inactivation*), while G_K remains activated. Reprinted by permission from Hodgkin (1958).

particles are independent, the probability for the three m and the one h particle to exist in this state is m^3h. Notice that h is the probability that the inactivating particle is *not* in its inactivating state. Formally, the temporal change of these particles is described by two first-order differential equations,

$$\frac{dm}{dt} = \alpha_m(V)(1 - m) - \beta_m(V)m \tag{6.14}$$

and

$$\frac{dh}{dt} = \alpha_h(V)(1 - h) - \beta_h(V)h\,. \tag{6.15}$$

Empirically, Hodgkin and Huxley derived the following equations for the rate constants:

$$\alpha_m(V) = \frac{25 - V}{10(e^{(25-V)/10} - 1)} \tag{6.16}$$

$$\beta_m(V) = 4e^{-V/18} \tag{6.17}$$

$$\alpha_h(V) = 0.07e^{-V/20} \tag{6.18}$$

$$\beta_h(V) = \frac{1}{e^{(30-V)/10} + 1}\,. \tag{6.19}$$

The associated time constants and steady-state variables are plotted in Fig. 6.3 as a function

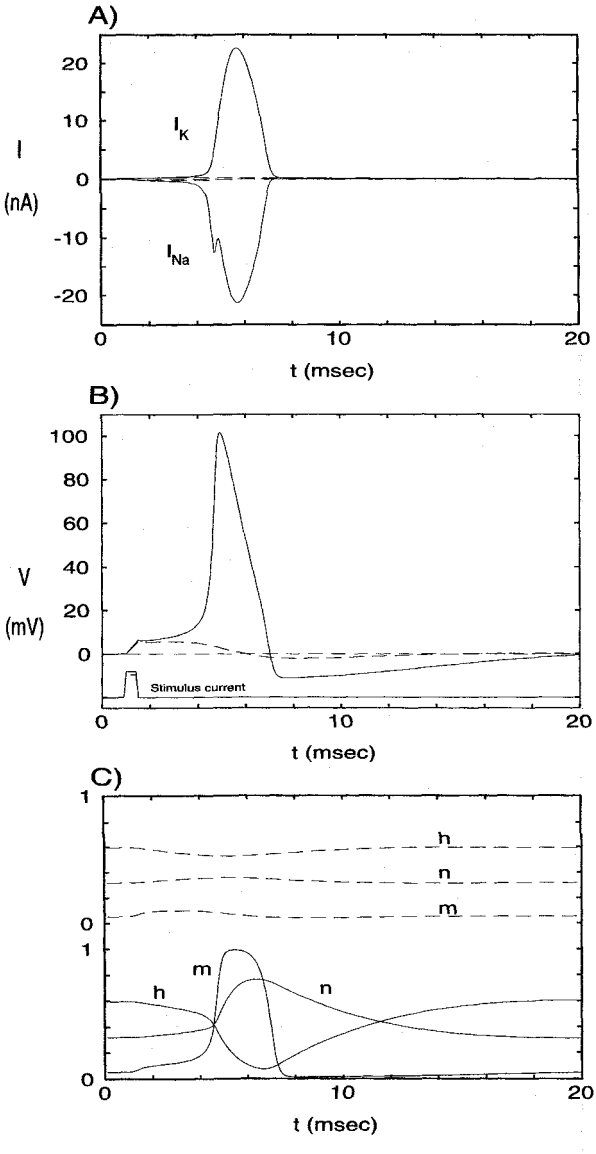

Fig. 6.5 HODGKIN-HUXLEY ACTION POTENTIAL Computed action potential in response to a 0.5-msec current pulse of 0.4-nA amplitude (solid lines) compared to a subthreshold response following a 0.35-nA current pulse (dashed lines). **(A)** Time course of the two ionic currents. Note their large sizes compared to the stimulating current. **(B)** Membrane potential in response to threshold and subthreshold stimuli. The injected current charges up the membrane capacity (with an effective membrane time constant $\tau = 0.85$ msec), enabling sufficient I_{Na} to be recruited to outweigh the increase in I_K (due to the increase in driving potential). The smaller current pulse fails to trigger an action potential, but causes a depolarization followed by a small hyperpolarization due to activation of I_K. **(C)** Dynamics of the gating particles. Sodium activation m changes much more rapidly than either h or n. The long time course of potassium activation n explains why the membrane potential takes 12 msec after the potential has first dipped below the resting potential to return to baseline level.

of voltage. Similar to before, both τ_m and τ_h are bell-shaped curves,[2] but with a tenfold difference in duration. While m_∞ is a monotonically increasing function of V, as expected of an activation variable, h_∞ decreases with increasing membrane depolarization, the defining feature of an inactivating particle. Without inactivation, the sodium conductance would remain at its maximum value in response to a depolarizing voltage step.

The fraction of the steady-state sodium conductance open at rest is less than 1% of the peak sodium conductance. Inspection of Fig. 6.3 immediately reveals the reason: for voltages below or close to the resting potential of the axon, the activation variable m is close to zero while at positive potentials the inactivation variable h is almost zero. Thus,

2. Note that the voltage-dependent membrane time constant for the activation variable τ_m has the same symbol as the passive membrane time constant. When in doubt, we will refer to the latter simply as τ.

the steady-state sodium current $\overline{G}_{Na} m_\infty^3 h_\infty (V - E_{Na})$, also known as the *window current*, is always very small. The secret to obtaining the large sodium current needed to rapidly depolarize the membrane lies in the temporal dynamics of m and h. At values of the membrane close to the resting potential, h takes on a value close to 1. When a sudden depolarizing voltage step is imposed onto the membrane as in Fig. 6.4, m changes within a fraction of a millisecond to its new value close to 1, while h requires 5 msec or longer to relax from its previous high value to its new and much smaller value. In other words, two processes control the sodium conductance: activation is the rapid process that increases G_{Na} upon depolarization and outpaces inactivation, the much slower process that reduces G_{Na} upon depolarization.

6.2.3 Complete Model

Similar to most other biological membranes, the axonal membrane contains a voltage-independent "leak" conductance G_m, which does not depend on the applied voltage and remains constant over time. The value measured by Hodgkin and Huxley, $G_m = 0.3\ \text{mS/cm}^2$, corresponds to a passive membrane resistivity of $R_m = 3333\ \Omega \cdot \text{cm}^2$. The passive component also has a reversal potential associated with it. Hodgkin and Huxley did not explicitly measure V_{rest}, but adjusted it so that the total membrane current at the resting potential $V = 0$ was zero. In other words, V_{rest} was defined via the equation $G_{Na}(0)E_{Na} + G_K(0)E_K + G_m V_{rest} = 0$, and came out to be +10.613 mV. The membrane capacity $C_m = 1\ \mu\text{F/cm}^2$. At the resting potential, the effective membrane resistance due to the presence of the sum of the leak, the potassium, and the (tiny) sodium conductances amounts to $857\ \Omega \cdot \text{cm}^2$, equivalent to an effective "passive" membrane time constant of about 0.85 msec.

We can now write down a single equation for all the currents flowing across a patch of axonal membrane,

$$C_m \frac{dV}{dt} = \overline{G}_{Na} m^3 h (E_{Na} - V) + \overline{G}_K n^4 (E_K - V) + G_m (V_{rest} - V) + I_{inj}(t) \quad (6.20)$$

where I_{inj} is the current that is injected via an intracellular electrode. This nonlinear differential equation, in addition to the three ordinary linear first-order differential equations specifying the evolution of the rate constants (as well as their voltage dependencies), constitutes the four-dimensional Hodgkin and Huxley model for the space-clamped axon or for a small patch of membrane. Throughout the book, we shall refer to Eq. 6.20, in combination with the rate constants (Eqs. 6.7, 6.14, and 6.15) at 6.3° C as the *standard Hodgkin-Huxley membrane patch model*. In our simulations of these equations, we solve Eq. 6.20 for an equipotential $30 \times 30 \times \pi\ \mu\text{m}^2$ patch of squid axonal membrane and therefore express I_m in units of nanoamperes (nA), and not as current density.

We will explain in the following sections how this model reproduces the stereotyped sequence of membrane events that give rise to the initiation and propagation of all-or-none action potentials.

6.3 Generation of Action Potentials

One of the most remarkable aspect of the axonal membrane is its propensity to respond in either of two ways to brief pulses of depolarizing inward current. If the amplitude of the pulse is below a given threshold, the membrane will depolarize slightly but will return to the

membrane's resting potential, while larger currents will induce a pulse-like action potential, whose overall shape is relatively independent of the stimulus required to trigger it.

Consider the effect of delivering a short (0.5-msec) inward current pulse $I_{inj}(t)$ of 0.35-nA amplitude to the membrane (Fig. 6.5). The injected current charges up the membrane capacitance, depolarizing the membrane in the process. The smaller this capacitance, the faster the potential will rise. The depolarization has the effect of slightly increasing m and n, in other words, increasing both sodium and potassium activation, but decreasing h, that is, decreasing potassium inactivation. Because the time constant of sodium activation is more than one order of magnitude faster than τ_n and τ_h at these voltages, we can consider the latter two for the moment to be stationary. But the sodium conductance G_{Na} will increase somewhat. Because the membrane is depolarized from rest, the driving potential for the potassium current, $V - E_K$, has also increased. The concomitant increase in I_K outweighs the increase in I_{Na} due to the increase in G_{Na} and the overall current is outward, driving the axon's potential back toward the resting potential. The membrane potential will slightly undershoot and then overshoot until it finally returns to V_{rest}. The oscillatory response around the resting potential can be attributed to the small-signal behavior of the potassium conductance acting phenomenologically similar to an inductance (see Chap. 10 for further discussion).

If the amplitude of the current pulse is increased slightly to 0.4 nA, the depolarization due to the voltage-independent membrane components will reach a point where the amount of I_{Na} generated exceeds the amount of I_K. At this point, the membrane voltage undergoes a runaway reaction: the additional I_{Na} depolarizes the membrane, further increasing m, which increases I_{Na}, causing further membrane depolarization. Given the almost instantaneous dynamics of sodium activation ($\tau_m \approx 0.1$–0.2 msec at these potentials), the inrushing sodium current moves the membrane potential within a fraction of a millisecond to 0 mV and beyond. In the absence of sodium inactivation and potassium activation, this positive feedback process would continue until the membrane would come to rest at E_{Na}. As we saw already in Fig. 6.4, after a delay both the slower sodium inactivation variable h as well as the potassium activation n will turn on (explaining why I_K is also called the *delayed rectifier* current I_{DR}). Sodium inactivation acts to directly decrease the amount of sodium conductance available, while the activation of the potassium conductance tends to try to bring the axon's membrane potential toward E_K by increasing I_K. Thus, both processes cause the membrane potential to dip down from its peak. Because the total sodium current quickly falls to zero after 1 msec, but I_K persists longer at small amplitudes (not readily visible in Fig. 6.5), the membrane potential is depressed to below its resting level, that is, the axon *hyperpolarizes*. At these low potentials, eventually potassium activation switches off, returning the system to its initial configuration as V approaches the resting potential.

6.3.1 Voltage Threshold for Spike Initiation

What are the exact conditions under which a spike is initiated? Does the voltage have to exceed a particular threshold value V_{th}, or does a minimal amount of current I_{th} have to be injected, or does a certain amount of electrical charge Q_{th} have to be delivered to the membrane in order to initiate spiking? These possibilities and more have been discussed in the literature and experimental evidence exists to support all of these views under different circumstances (Hodgkin and Rushton, 1946; Cooley, Dodge, and Cohen, 1965; Noble and Stein, 1966; Cole, 1972; Rinzel, 1978; for a thorough discussion see Jack, Noble, and Tsien, 1975). Because the squid axon is not a good model for spike encoding in central neurons,

we will defer a more detailed discussion of this issue to Secs. 17.3 and 19.2. We here limit ourselves to considering spike initiation in an idealized nonlinear membrane, without dealing with the complications of cable structures (such as the axon).

To answer this question, we need to consider the I–V relationship of the squid axonal membrane. Because we are interested in rapid synaptic inputs, we assume that the risetime of the synaptic current is faster than the effective passive time constant, $\tau = 0.85$ msec, and make use of the observation that the dynamics of sodium activation m is very rapid (the associated time constant is always less than 0.5 msec) and at least a factor of 10 faster than sodium inactivation h and potassium activation n (see Fig. 6.3). With these observations in mind, we ask what happens if the input depolarizes the membrane very rapidly to a new value V? Let us estimate the current that will flow with the help of the *instantaneous* I–V relationship $I_0(V)$ (Fig. 6.6).

I_0 is given by the sum of the ionic and the leak currents. We approximate the associated sodium and potassium conductances by assuming that h and n have not had time to change from the value they had at the resting potential $V = 0$, while m adjusts instantaneously to its new value at V. In other words,

$$I_0(V) = \overline{G}_{\mathrm{Na}} m(V)^3 h(0)(V - E_{\mathrm{Na}}) + \overline{G}_{\mathrm{K}} n(0)^4 (V - E_{\mathrm{K}}) + G_m (V - V_{\mathrm{rest}}) \quad (6.21)$$

Figure 6.6 shows the inverted U-form shape of I_0 in the neighborhood of the resting potential, as well as its three ionic components I_{Na}, I_{K}, and I_{leak}.

In the absence of any input, the system rests at $V = 0$. If a small depolarizing voltage step is applied, the system is displaced to the right, generating a small, positive current. This current is outward since the increase in m (increasing the amplitude of I_{Na}) is outweighed by the increase in the driving potential $V - E_{\mathrm{K}}$ (increasing I_{K}) and the decrease in I_{leak}.

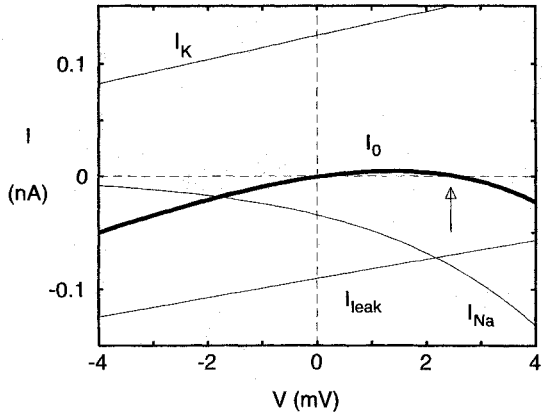

Fig. 6.6 Current-Voltage Relationship around Rest Instantaneous I–V relationship, I_0, associated with the standard patch of squid axon membrane and its three components: $I_0 = I_{\mathrm{Na}} + I_{\mathrm{K}} + I_{\mathrm{leak}}$ (Eq. 6.21). Because m changes much faster than either h or n for rapid inputs, we computed G_{Na} and G_{K} under the assumption that m adapts instantaneously to its new value at V, while h and n remain at their resting values. I_0 crosses the voltage axis at two points: a stable point at $V = 0$ and an unstable one at $V_{\mathrm{th}} \approx 2.5$ mV. Under these idealized conditions, any input that exceeds V_{th} will lead to a spike. For the "real" equations, m does not change instantaneously and nor do n and h remain stationary; thus, I_0 only crudely predicts the voltage threshold which is, in fact, 6.85 mV for rapid synaptic input. Note that I_0 is specified in absolute terms and scales with the size of the membrane patch.

This forces the membrane potential back down toward the resting potential: the voltage trajectory corresponds to a subthreshold input. Similarly, if a hyperpolarizing current step is injected, moving the system to below $V = 0$, a negative inward current is generated, pulling the membrane back up toward V_{rest}. The slope of the I–V curve around the resting potential $\partial I/\partial V$, termed the *membrane slope conductance*, is positive (for a substantial discussion of this concept, see Sec. 17.1.2). That is, the point $V = 0$ is a *stable attractor*. (For these and related notions, we defer the reader to the following chapter.)

$I_0(V)$ has a second zero crossing at $V = V_{\text{th}} \approx 2.5$ mV. If an input moves the membrane potential to exactly V_{th}, no current flows and the system remains at V_{th} (Fig. 6.6). Because the slope conductance is negative, the point is unstable, and an arbitrarily small perturbation will carry the system away from the zero crossing. A negative perturbation will carry the system back to V_{rest}. Conversely, a positive voltage displacement, no matter how minute, causes a small inward current to flow, which further depolarizes the membrane (due to the negative slope conductance), leading in turn to a larger inward current, and so on. The membrane potential rapidly increases to above absolute zero, that is, an action potential is triggered. During this phase, very large inward currents are generated, far exceeding the amplitude of the modest stimulus current. (Recall that around these potentials, I_{Na} increases e-fold every 3.9 mV.) For the patch of squid membrane simulated here (where the current scales linearly with the area of the patch), the peak of I_{Na} is about 23 nA.

This qualitative account of the origin of the voltage threshold for an active patch of membrane argues that in order for an action potential to be initiated, the net inward current must be negative. For rapid input, this first occurs at $V = V_{\text{th}}$. This analysis was based on the rather restrictive assumption that m changes instantaneously, while h and n remain fixed. In practice, neither assumption is perfect. Indeed, while our argument predicts $V_{\text{th}} = 2.5$ mV, the voltage threshold for spike initiation for rapid EPSPs for the Hodgkin–Huxley equation is, in fact, equal to 6.85 mV (Noble and Stein, 1966). As discussed in Sec. 17.3, reaching a particular value of the voltage for a rapid input in a single compartment is equivalent to rapidly dumping a threshold amount of charge Q_{th} into the system.

Applying a current step that increases very slowly in amplitude—allowing the system to relax always to its stationary state—prevents any substantial sodium current from flowing and will therefore not cause spiking. Thus, not only does a given voltage level have to be reached and exceeded but also within a given time window. We take up this issue in Sec. 17.3 in the context of our full pyramidal cell model and in Sec. 19.2 to explore how V_{th} is affected by the cable structure.

6.3.2 Refractory Period

Once the rapid upstroke exceeding 0 has been generated, the membrane potential should be pulled back to its resting potential, that is, repolarized, as rapidly as possible in order to enable the system to generate the next impulse.[3]

This is accomplished by inactivating G_{Na} and by increasing a potassium conductance, G_{K}. This conductance remains activated even subsequent to spike polarization (for up to 12 msec following the peak of the action potential in Fig. 6.5), causing the membrane to undergo a hyperpolarization. During this period, it is more difficult to initiate an action potential than before; the membrane remains in a *refractory* state. The reason for the reduced ability of the membrane to discharge again is the inactivation of I_{Na} (that is, h is small) and the continuing activation of I_{K} (n only decays slowly).

3. Given a specific membrane capacitance of 1 μF/cm^2, the 100 mV spike depolarization amounts to transferring about 6,000 positively charged ions per μm^2 of membrane area.

This *refractory period* can be documented by the use of a second current pulse (Fig. 6.7). At $t = 1$ msec a 0.5-msec current pulse is injected into our standard patch of squid axonal membrane. The amplitude of this pulse, $I_1 = 3.95$ nA, is close to the minimal one needed to generate an action potential. The input causes a spike to be triggered that peaks at around 5 msec and repolarizes to $V = 0$ at $t = 7$ msec. This time, at which the membrane potential starts to dip below the resting potential (Fig. 6.5), is somewhat arbitrarily assigned to $\Delta t = 0$. Following this point, a second 0.5-msec-long current pulse of amplitude I_2 is applied Δt msec later. The amplitude of I_2 is increased until a second action potential is generated. This first occurs at $\Delta t = 2$ msec (that is, 2 msec after the membrane potential has repolarized to zero). At this time, $I_2/I_1 = 23.7$, that is, the amplitude of the second pulse must be 23.7 times larger than the amplitude of the first pulse in order to trigger a spike. Since such large current amplitudes are unphysiological, the membrane is *de facto* not excitable during this period, which is frequently referred to as the *absolute refractory period.* The threshold for initiation of the second spike is elevated up to 11 msec after repolarization of the membrane due to the first spike (*relative refractory period*; Fig. 6.7). This is followed by a brief period of mild hyperexcitability, when a spike can be elicited by a slightly (15%) smaller current than under resting conditions.

From a computational point of view, it is important to realize that the threshold behavior of the Hodgkin–Huxley model depends on the previous spiking history of the membrane. In the squid axon, as in most axons, the threshold rises only briefly, returning to baseline levels after 20 msec or less. As warming the axon to body temperatures speeds up the rates of gating two- to fourfold,[4] the minimal separation time is expected to be only 1–2 msec

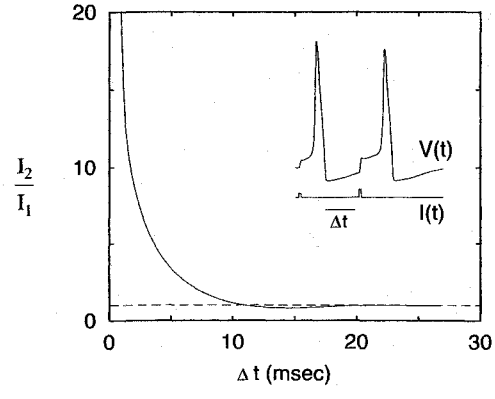

Fig. 6.7 Refractory Period A 0.5-msec brief current pulse of $I_1 = 0.4$ nA amplitude causes an action potential (Fig. 6.5). A second, equally brief pulse of amplitude I_2 is injected Δt msec after the membrane potential due to the first spike having reached $V = 0$ and is about to hyperpolarize the membrane. For each value of Δt, I_2 is increased until a second spike is generated (see the inset for $\Delta t = 10$ msec). The ratio I_2/I_1 of the two pulses is here plotted as a function of Δt. For several milliseconds following repolarization, the membrane is practically inexcitable since such large currents are unphysiological (*absolute refractory period*). Subsequently, a spike can be generated, but it requires a larger current input (*relative refractory period*). This is followed by a brief period of reduced threshold (hyperexcitability). No more interactions are observed beyond about $\Delta t = 18$ msec.

4. A crucial parameter in determining the dynamics of the action potential is the temperature. As first mentioned in footnote 5 in Sec. 4.6, if the temperature is reduced, the rate at which the ionic channels underlying the action potential open or close slows down, while the peak conductance remains unchanged. Hodgkin and Huxley recorded most of their data at 6.3° C and the rate constants are expressed at these temperatures (Eqs. 6.10, 6.11 and 6.16–6.19). To obtain the action potential at any other temperature T, all α's and β's need to be corrected by $Q_{10}^{(T-6.3)/10}$, with Q_{10} between 2 and 4 (Hodgkin, Huxley, and Katz, 1952;

for axons in warm-blooded animals. Nerve cells—as compared to axons—often display a much longer increase in their effective spiking threshold, depending on the number of action potentials generated within the last 100 msec or longer (Raymond, 1979). Section 9.3 will treat the biophysical mechanism underlying this short-term *firing frequency adaptation* in more detail.

6.4 Relating Firing Frequency to Sustained Current Input

What happens if a long-lasting current step of constant amplitude is injected into the space-clamped axon (Agin, 1964; Cooley, Dodge, and Cohen, 1965; Stein, 1967a)? If the current is too small, it will give rise to a persistent subthreshold depolarization (Fig. 6.8). Plotting the steady-state membrane depolarization as a function of the applied membrane current (Fig. 6.9A) reveals the linear relationship between the two. If the input is of sufficient amplitude to exceed the threshold, the membrane will generate a single action potential (Fig. 6.8). The minimal amount of sustained current needed to generate at least one action potential (but not necessarily an infinite train of spikes) is called *rheobase* (Cole, 1972). For our standard membrane patch, rheobase corresponds to 0.065 nA. (This current is obviously far less than the amplitude of the brief current pulse used previously.) After the spike has been trigged and following the afterhyperpolarization, $V(t)$ stabilizes at around 2 mV positive to the resting potential, limiting the removal of sodium inactivation as well as enhancing I_K. As the current amplitude is increased, the offset depolarization following the action potential and its hyperpolarization increases until, when the amplitude of the current step is about three times rheobase (0.175 nA), a second action potential is initiated. At around 0.18 nA (I_1 in Fig. 6.9A), the Hodgkin–Huxley equations will start to generate an indefinite train of spikes, that is, the membrane fires repetitively. After the membrane potential goes through its gyrations following each action potential, V creeps past V_{th} and the cycle begins anew: the system travels on a stable limit cycle. In a noiseless situation, the interval between consecutive spikes is constant and the cell behaves as a periodic oscillator with constant frequency.

Figure 6.9A shows the associated steady-state I–V relationship. Experimentally, it can be obtained by clamping the membrane potential to a particular value V and measuring the resultant clamp current I. The equations generate infinite trains of action potentials for $I \geq I_1$ (dashed line in Fig. 6.9A).

A mathematical curiosity of uncertain relevance is the observation that for a range of amplitudes of the current step, the Hodgkin–Huxley equations can display several solutions, including the stable and periodic oscillation emphasized here, a stable but steady-state depolarizing solution, and an unstable periodic solution (Troy, 1978; Rinzel and Miller, 1980). Which one is actually realized depends on the initial conditions.

If the current amplitude is further increased, the interspike intervals begin to decrease and the spiking frequency increases. Figure 6.9B shows the relationship between the amplitude of the injected current and the spiking frequency around threshold, and Fig. 6.10A over a larger current range. It is referred to as the *frequency–current* or f–I curve. Overall,

(continued) Beam and Donaldson, 1983; for a definition of Q_{10} see footnote 5 in Sec. 4.6). The Q_{10} for the peak conductances is a modest 1.3. As the temperature is increased, the *upstroke*, that is, the rate at which the voltage rises during the rapid depolarizing phase of the action potential, increases, because the speed at which I_{Na} is activated increases. At the same time, both sodium inactivation and potassium activation increase. Altogether, the total duration of the spike decreases. At temperatures above 33° C no spike is generated (Hodgkin and Katz, 1949; of course, the squid axon lives in far more frigid waters than these balmy temperatures).

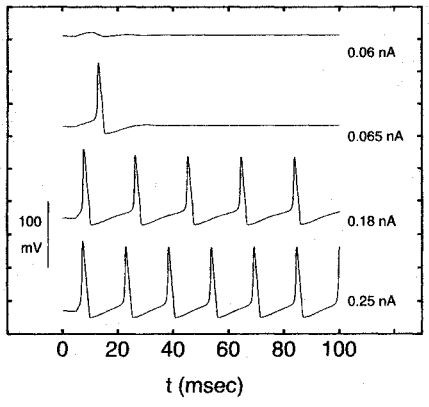

Fig. 6.8 REPETITIVE SPIKING Voltage trajectories in response to current steps of various amplitudes in the standard patch of squid axonal membrane. The minimum sustained current necessary to initiate a spike, termed *rheobase*, is 0.065 nA. In order for the membrane to spike indefinitely, larger currents must be used. Experimentally, the squid axon usually stops firing after a few seconds due to secondary inactivation processes not modeled by the Hodgkin–Huxley equations (1952d).

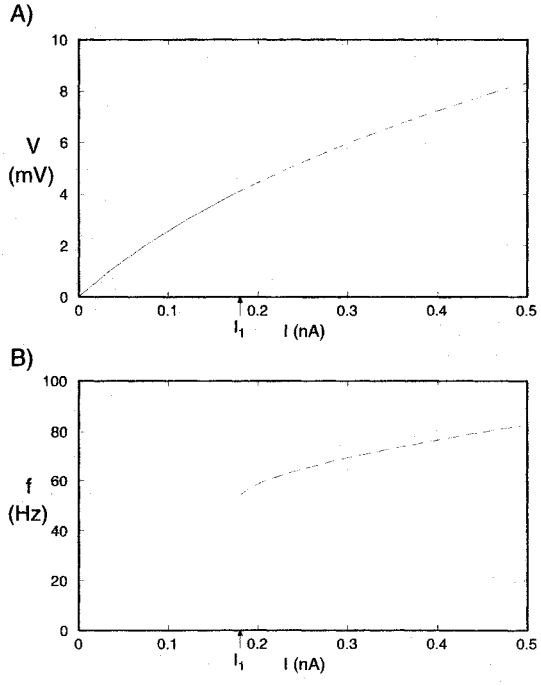

Fig. 6.9 SUSTAINED SPIKING IN THE HODGKIN-HUXLEY EQUATIONS **(A)** Steady-state I–V relationship and **(B)** f–I or discharge curve as a function of the amplitude of the sustained current I associated with the Hodgkin-Huxley equations for a patch of squid axonal membrane. For currents less than 0.18 nA, the membrane responds by a sustained depolarization (solid curve). At I_1, the system loses its stability and generates an infinite train of action potentials: it moves along a stable limit cycle (dashed line). A characteristic feature of the squid membrane is its abrupt onset of firing with nonzero oscillation frequency. The steady-state I–V curve can also be viewed as the sum of all steady-state ionic currents flowing at any particular membrane potential V_m.

there is a fairly limited range of frequencies at which the membrane fires, between 53 and 138 Hz. If a current at the upper amplitude range is injected in the axon, the membrane fails to repolarize sufficiently between spikes to relieve sodium inactivation. Thus, although

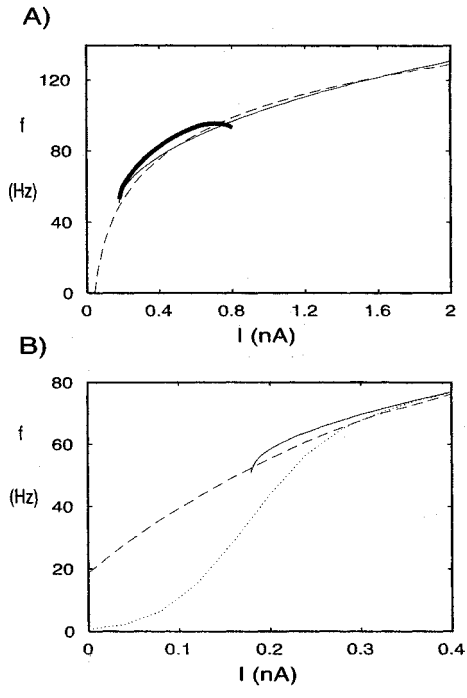

Fig. 6.10 HODGKIN-HUXLEY f–I CURVE AND NOISE **(A)** Relationship between the amplitude of an injected current step and the frequency of the resultant sustained discharge of action potentials (f–I curve) for a membrane patch of squid axon at 6.3° C (solid line) and its numerical fit (dashed line) by $f = 33.2 \log I + 106$. Superimposed in bold is the f–I curve for the standard squid axon cable (using normalized current). Notice the very limited bandwidth of axonal firing. **(B)** f–I curve for the membrane patch case around its threshold (rheobase) in the presence of noise. White (2000-Hz band-limited) current noise whose amplitude is Gaussian distributed with zero mean current is added to the current stimulus. In the absence of any noise (solid line) the f–I curve shows abrupt onset of spiking. The effect of noise (dotted curve—standard deviation of 0.05 nA; dashed curve—0.1 nA) is to linearize the threshold behavior and to increase the bandwidth of transmission (stochastic linearization). Linear f–I curves are also obtained when replacing the continuous and deterministic Hodgkin-Huxley currents by discrete and stochastic channels (see Sec. 8.3).

the membrane potential does show oscillatory behavior, no true action potentials are generated.

In the laboratory, maintained firing in the squid axon is not that common (Hagiwara and Oomura, 1958; see, however, Chapman, 1963). This is most likely due to secondary inactivation mechanisms which are not incorporated into the Hodgkin–Huxley equations. Yet for short times, the theoretical model of Hodgkin and Huxley makes reasonably satisfactory predictions of the behavior of the space-clamped axon (for a detailed comparison between experimental observations and theoretical predictions see Guttman and Barnhill, 1970 as well as Chap. 11 in the ever trustworthy Jack, Noble, and Tsien, 1975), in particular with respect to the small dynamic range of firing frequencies supported by the axonal membrane and the abrupt onset of spiking at a high firing frequency. The f–I curve can be well approximated by either a square root or a logarithmic relationship between frequency and injected current (Agin, 1964; see Fig. 6.10).

The f–I curves of most neurons, and not just the squid axon, bend over and saturate for large input currents. This justifies the introduction of a smooth, sigmoidal nonlinearity

mimicking the neuronal input-output transduction process in continuously valued neural network models (Hopfield, 1984). It is important to keep in mind that the paradigm under which the f–I curves are obtained, sustained current input, represents only a very crude approximation to the dynamic events occurring during synaptic bombardment of a cell leading to very complex spike discharge patterns (see Chap. 14).

An important feature of the Hodgkin–Huxley model is that the frequency at the onset of repetitive activity has a well-defined nonzero minimum (about 53 Hz at 6.3° C; Fig. 6.10B). The membrane is not able to sustain oscillations at lower frequencies. This behavior, generated by a so-called *Hopf bifurcation* mechanism, is generic to a large class of oscillators occurring in nonlinear differential equations (Cronin, 1987; Rinzel and Ermentrout, 1998) and will be treated in more detail in the following chapter.

As first explicitly simulated by Stein (1967b), adding random variability to the input can increase the bandwidth of the axon by effectively increasing the range within which the membrane can generate action potentials. If the input current is made to vary around its mean with some variance, reflecting for instance the spontaneous release of synaptic vesicles, the sharp discontinuity in the firing frequency at low current amplitudes is eliminated, since even with an input current that is on average below threshold, the stimulus will become strong enough to generate an impulse with a finite, though small, average frequency. Depending on the level of noise, the effective minimal firing frequency can be reduced to close to zero (Fig. 6.10B). A similar linearization behavior can be obtained if the continuous, deterministic, and macroscopic currents inherent in the Hodgkin–Huxley equations are approximated by the underlying discrete, stochastic, and microscopic channels (Skaugen and Walloe, 1979; see Sec. 8.3).

Adding noise to a quantized signal to reduce the effect of this discretization is a standard technique in engineering known as *dithering* or *stochastic linearization* (Gammaitoni, 1995; Stemmler, 1996).

A large number of neurons can generate repetitive spike trains with arbitrarily small frequencies. As first shown by Connor and Stevens (1971c) in their Hodgkin–Huxley-like model of a gastropod nerve cell, the addition of a transient, inactivating potassium current (termed the I_A current) enables the cell to respond to very small sustained input currents with a maintained discharge of very low frequency. (This topic will be further pursued in Sec. 7.2.2.) Such low firing frequencies are also supported by pyramidal cells (Fig. 9.7).

6.5 Action Potential Propagation along the Axon

Once the threshold for excitation has been exceeded, the all-or-none action potential can propagate from the stimulus site to other areas of the axon. The hypothesis that this propagation is mediated by cable currents flowing from excited to neighboring, nonexcited regions was suggested already around the turn of the century by Hermann (1899). It was not until Hodgkin (1937) that direct experimental proof became available. A quantitative theory of this propagation had to await Hodgkin and Huxley's 1952 study. Because this has been a very well explored chapter in the history of biophysics, we will be brief here, only summarizing the salient points. Chapter 10 in Jack, Noble, and Tsien (1975) provides a deep and thorough coverage of nonlinear cable theory as applied to the conduction of action potentials. Section 19.2 will deal with how cable structures, such as an infinite cylinder, affect the voltage threshold for spike initiation.

6.5.1 Empirical Determination of the Propagation Velocity

The equivalent electrical circuit replicates the patch of sodium, potassium, and leak conductances and batteries (Fig. 6.2) along the cable in a fashion we are already familiar with from the passive cable (Fig. 6.11). Equation 2.5 specifies the relationship between the membrane current (per unit length) and the voltage along the cable,

$$i_m = \frac{1}{r_a}\frac{\partial^2 V}{\partial x^2}. \tag{6.22}$$

In Eq. 6.20, we derived the membrane current (per unit area) flowing in a patch of axonal membrane. Combining the two with the appropriate attention to scaling factors leads to an equation relating the potential along the axon to the electrical property of the active membrane,

$$\frac{d}{4R_i}\frac{\partial^2 V}{\partial x^2} = C_m\frac{\partial V}{\partial t} + \overline{G}_{\mathrm{Na}}m^3h(V - E_{\mathrm{Na}}) + \overline{G}_{\mathrm{K}}n^4(V - E_{\mathrm{K}}) + G_m(V - V_{\mathrm{rest}}) \tag{6.23}$$

where d is the diameter of the axon. Hodgkin and Huxley (1952d) used a $d = 0.476$ mm thick axon in their calculations and a value of $R_i = 35.4\ \Omega\cdot$cm. This nonlinear partial differential equation, in conjunction with the three equations describing the dynamics of m, h, and n and the appropriate initial and boundary conditions, constitutes the complete Hodgkin–Huxley model.

This type of second-order equation, for which no general analytical solution is known, is called a *reaction-diffusion* equation, because it can be put into the form of

$$\frac{\partial V}{\partial t} = D\frac{\partial^2 V}{\partial x^2} + F(V) \tag{6.24}$$

with $D > 0$ constant. We will meet this type of equation again when considering the dynamics of intracellular calcium (see Chap. 11). Under certain conditions, it has wave-like solutions.

Because Hodgkin and Huxley only had access to a very primitive hand calculator, they could not directly solve Eq. 6.23. Instead, they considered a particular solution to these equations. Since they observed that the action potential propagated along the axon without changing its shape, they postulated the existence of a wave solution to this equation, in which the action potential travels with constant velocity u along the axon, that is, $V(x, t) = V(x - ut)$. Taking the second spatial and temporal derivative of this

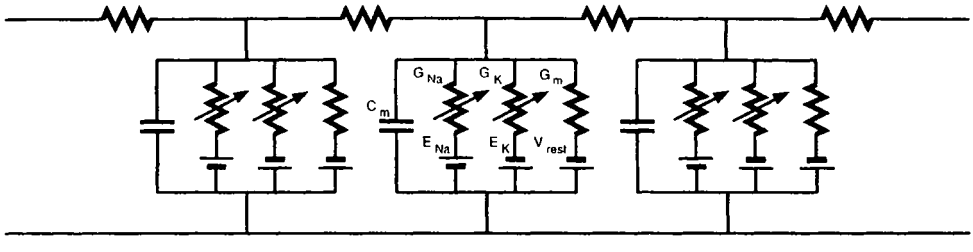

Fig. 6.11 Electrical Circuit of the Squid Giant Axon One-dimensional cable model of the squid giant axon. The structure of the cable is as in the passive case (Fig. 2.2B), with the *RC* membrane components augmented with circuit elements modeling the sodium and potassium currents (Fig. 6.2).

expression and using the chain rule leads to a second-order hyperbolic partial differential equation,

$$\frac{\partial^2 V}{\partial x^2} = \frac{1}{u^2}\frac{\partial^2 V}{\partial t^2}. \tag{6.25}$$

Replacing the second spatial derivative term in Eq. 6.23 with this expression yields

$$\frac{1}{K}\frac{d^2 V}{dt^2} = \frac{dV}{dt} + \frac{I_{\text{ionic}}}{C_m} \tag{6.26}$$

with $K = 4R_i u^2 C_m/d$ and I_{ionic} defined in Eq. 6.2. Equation 6.26 is an ordinary second-order differential equation, whose solution is much easier to compute than the solution to the full-blown partial differential equation. It does require, though, a value for u. By a laborious trial-and-error procedure, Hodgkin and Huxley iteratively solved this equation until they found a value of u leading to a stable propagating wave solution. In a truly remarkable test of the power of their model, they estimated 18.8 m/sec (at 18.3° C) for the velocity at which the spike propagates along the squid giant axon, a value within 10% of the experimental value of 21.2 m/sec. This is all the more remarkable, given that their model is based on voltage- and space-clamped data, and represents one of the rare instances in which a neurobiological model makes a successful quantitative prediction.

We can establish the dependency of the velocity on the diameter of the fiber using the following argumentation. Because both I_i and C_m are expressed as current and capacitance per unit membrane area, their ratio is independent of the fiber diameter. The voltage across the membrane and its temporal derivatives must also be independent of d. This implies that the constant K in Eq. 6.26 must remain invariant to changes in diameter. Assuming that C_m and R_i do not depend on d, we are lead to the conclusion that the velocity u must be

$$u \propto \sqrt{d}. \tag{6.27}$$

In other words, the propagation velocity in unmyelinated fibers is expected to be proportional to the square root of the axonal diameter.[5] Indeed, this predicted relationship is roughly followed in real neurons (see Fig. 6.16; Ritchie, 1995).

This implies that if the delay between spike initiation at the cell body and the arrival of the spike at the termination of an axon needs to be cut in half, the diameter of the axon needs to increase by a factor of 4, a heavy price to pay for rapid communication. The premium put on minimizing propagation delay in long cable structures is most likely the reason the squid evolved such thick axons. As we will see further below, many axons in vertebrates use a particular form of electrical insulation, termed *myelination*, to greatly speed up spike propagation without a concomitant increase in fiber diameter.

It was more than 10 years later that Cooley, Dodge, and Cohen (1965; see also Cooley and Dodge, 1966) solved the full partial differential equation (Eq. 6.23) numerically using an iterative technique. Figure 6.12 displays the voltage trajectory at three different locations along the axon; at $x = 0$ a short suprathreshold current pulse charges up the local membrane capacitance. This activates the sodium conductance and Na^+ ions rush in, initiating the full-blown action potential (not shown). The local circuit current generated by this spike leads to an exponential rise in the membrane potential in the neighboring region, known as the "foot" of the action potential. This capacitive current in turn activates the local sodium conductance, which will increase rapidly, bringing this region above threshold:

5. Notice that we derived a similar square-root relationship between diameter and "pseudovelocity" for the decremental wave in the case of a passive cable (Eq. 2.53).

the spike propagates along the axon. Different from the space-clamped axon, where the capacitive current is always equal and opposite to the ionic currents once the stimulus current has stopped flowing (Eq. 6.20), the time course of current is more complex during the propagated action potential due to the local circuit currents. Because some fraction of the local membrane current depolarizes neighboring segments of the axonal cable (the so-called *local circuit* currents; see Fig. 6.13), the current amplitude required to trigger at least one action potential is larger than the current amplitude in the space-clamped case

If the voltage applied to the squid membrane is small enough, one can *linearize* the membrane, describing its behavior in terms of voltage-independent resistances, capacitances, and inductances. This procedure was first carried out by Hodgkin and Huxley (1952d) and will be discussed in detail in Chap. 10. Under these circumstances, a space constant λ can be associated with the "linearized" cable, describing how very small currents are attenuated along the axon. At rest, the dc space constant for the squid axon is $\lambda = 5.4$ mm, about 10 times larger than its diameter.

When long current steps of varying amplitudes are injected into the axon, the squid axon responds with regular, periodic spikes. However, the already small dynamic range of the f–I curve of the space-clamped axon (Fig. 6.10A) becomes further reduced to a factor of less than 1.7 when the sustained firing activity in the full axon is considered (from 58 to 96 Hz at 6.3° C). Thus, while the Hodgkin–Huxley model describes to a remarkable degree the behavior of the squid's giant axon, the equations do not serve as an adequate model for impulse transduction in nerve cells, most of which have a dynamic range that extends over two orders of magnitude.

As predicted by Huxley (1959), Cooley and Dodge (1966) found a second solution to the Hodgkin–Huxley equations. When the amplitude of the injected current step is very close to the threshold for spike initiation, they observed a decremental wave propagating away

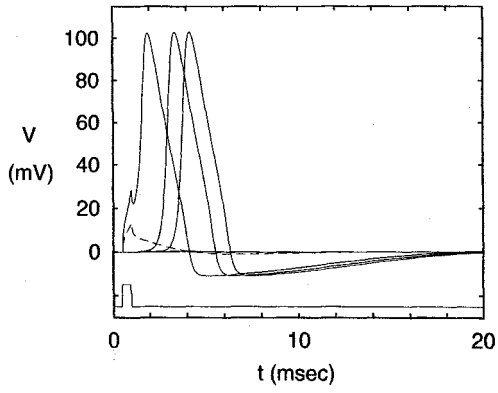

Fig. 6.12 PROPAGATING ACTION POTENTIAL Solution to the complete Hodgkin–Huxley model for a 5-cm-long piece of squid axon for a brief suprathreshold current pulse delivered to one end of the axon. This pulse generates an action potential that travels down the cable and is shown here at the origin as well as 2 and 3 cm away from the stimulating electrode (solid lines). Notice that the shape of the action potential remains invariant due to the nonlinear membrane. The effective velocity of the spike is 12.3 m/sec (at 6.3° C). If the amplitude of the current pulse is halved, only a local depolarization is generated (dashed curve) that depolarizes the membrane 2 cm away by a mere 0.5 mV (not shown). This illustrates the dramatic difference between active and passive voltage propagation.

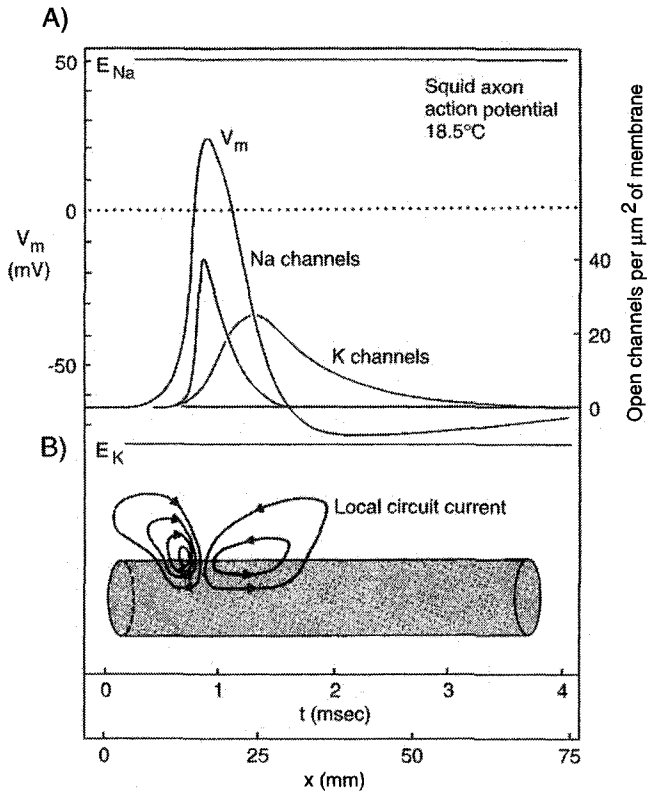

Fig. 6.13 Local Circuit Current in the Squid Axon Illustration of the events occurring in the squid axon during the propagation of an action potential. Since the spike behaves like a wave traveling at constant velocity, these two panels can be thought of either as showing the voltages and currents in time at one location or as providing a snapshot of the state of the axon at one particular instant (see the space/time axes at the bottom). **(A)** Distribution of the voltage (left scale) or the number of open channels (right scale) as inferred from the Hodgkin–Huxley model at 18.5° C. **(B)** *Local circuit currents* that spread from an excited patch of the axon to neighboring regions bringing them above threshold, thereby propagating the action potential. The diameter of the axon (0.476 mm) is not drawn to scale. Reprinted by permission from Hille (1992).

from the source. This solution quickly dies away to zero potential as x increases and is only observed if the amplitude of the current step is within 0.1% of the threshold current needed to obtain at least one spike. This phenomenon reveals the fact that the Hodgkin–Huxley model does not possess a strict threshold in the true sense of the word. In other words, there exists a continuous transformation between the subthreshold and the threshold voltage response. Yet in order to reveal these intermediate solutions the excitation must be adjusted with a degree of accuracy impossible to achieve physiologically. Practically speaking, given unavoidable noise in any neuronal system, only the propagating wave solution (with its associated threshold) plays a significant role in propagating information along the axon.

Cooley and Dodge (1966) also considered what happens if the density of voltage-dependent channels underlying G_{Na} and G_K is attenuated by a factor of η (with $0 \leq \eta \leq 1$; the value of V_{rest} and G_{leak} were adjusted so that the resting potential and resting conductance

were held constant). Reducing these conductances is somewhat analogous to the action of certain local anesthetics, such as lidocaine or procaine as used by dentists, in blocking action potential propagation. As η is reduced below 1, the velocity of propagation as well as the peak amplitude of the spike are reduced. For $\eta < 0.26$, no uniform wave solution is possible and the "action potential" decrements with distance.

6.5.2 Nonlinear Wave Propagation

Spikes moving down an axon are but one instance of a *nonlinear propagating wave*—nonlinear since in a linear dispersive medium, such as a passive cable, the different Fourier components associated with any particular voltage disturbance will propagate at a different velocity and the disturbance will lose its shape. This is why propagating spikes and the like are frequently referred to by mathematicians as resulting from *nonlinear diffusion*. Other examples include sonic shock waves or the digital pulses in an optical cable.

Scott (1975) argues for a broad classification of such phenomena into (1) those systems for which energy is conserved and which obey a conservation law and (2) those for which solitary traveling waves imply a balance between the rate of energy release by some nonlinearity and its consumption.

Waves associated with the first type of systems are known as *solitons* and are always based on energy conservation (Scott, Chu, and McLaughlin, 1973). Solitons emerge from a balance between the effects of nonlinearity, which tend to draw the wave together, fighting dispersion, which tends to spread the pulse out. This implies that solitons can propagate over a range of speeds. Furthermore, they can propagate through each other without any interference. Solitons have been observed in ocean waves and play a major role in high-speed optical fibers.

Action potentials are an example of the second type of propagating wave, similar to an ordinary burning candle (Scott, 1975). Diffusion of heat down the candle releases wax which burns to supply the heat. If P is the power (in joules per second) necesssary to feed the flame and E the chemical energy stored per unit length of the candle (joules per meter), the nonlinear wave in the form of the flame moves down the candle at a fixed velocity u given by

$$P = uE . \tag{6.28}$$

In other words, the velocity is fixed by the properties of the medium and does not depend on the initial conditions. Were we to light flames at both ends of a candle, the flames would move toward each other and annihilate themselves. This is also true if action potentials are initiated at the opposite ends of an axon. When they meet, they run into each other's refractory period and destroy each other. Thus, spikes are not solitons.

6.6 Action Potential Propagation in Myelinated Fibers

The successful culmination of the research effort by Hodgkin and Huxley heralded the coming of age of neurobiology. While we will deal in Chap. 9 with their methodology as applied in the past decades to the ionic currents found at the cell body of nerve cells, let us here briefly summarize spike propagation in *myelinated* axons (for more details, see Waxman, Kocsis, and Stys, 1995; Ritchie, 1995; Weiss, 1996).

Axons come in two flavors, those covered by layers of the lipid *myelin* and those that are not. The squid axon is an unmyelinated fiber, common to invertebrates. In vertebrates, many

fibers are wrapped dozens or even hundreds of times with myelin, the actual diameter of the axon itself being only 60% or 70% of the total diameter (Fig. 6.14). This insulating material is formed by special supporting cells, called *Schwann* cells in the peripheral nervous system and *oligodendrocytes* in the central nervous system.

A second specialization of myelinated fibers is that the myelin sheet is interrupted at regular intervals along the axon by nodes, named for their discoverer *nodes of Ranvier*. Here, the extracellular space gains direct access to the axonal membrane. Typically, the length of a node is very small (0.1%) compared to the length of the *internodal* segment (Fig. 6.15). In the vertebrate, single myelinated fibers range in diameter from 0.2 to 20 μm, while unmyelinated fibers range between 0.1 and 1 μm. In stark contrast, the diameters of unmyelinated invertebrate fibers range from under 1 μm to 1 mm.

In myelinated axons, conduction does not proceed continuously along the cable, but jumps in a discontinuous manner from one node to the next. This *saltatory conduction* (from the Latin *saltus*, to leap) was clearly demonstrated by Huxley and Stämpfli (1949) and Tasaki (1953). What these and similar experiments on frog, rabbit, and rat myelinated fibers made clear is that ionic currents are strikingly inhomogeneously distributed across the axonal membrane (Fig. 6.15; FitzHugh, 1962; Frankenhaeuser and Huxley, 1964; Stämpfli and Hille, 1976; Rogart and Ritchie, 1977; Chiu et al., 1979; Chiu and Ritchie, 1980). Spike generation essentially only takes place at the small nodes of Ranvier, which are loaded with fast sodium channels (between 700 and 2000 per square micrometer). In mammalian myelinated nerves, the repolarization of the spike is not driven by a large outward potassium current, as in the squid axon[6] but is achieved using a rapid sodium inactivation in combination with a large effective leak conductance. Indeed, action potentials do not show any hyperpolarization (Fig. 6.1B), unlike those in the squid giant axon. The origin of the large voltage-independent leak might involve an extracellular pathway beneath the myelin that connects the nodal and internodal regions (Barrett and Barrett, 1982; Ritchie,

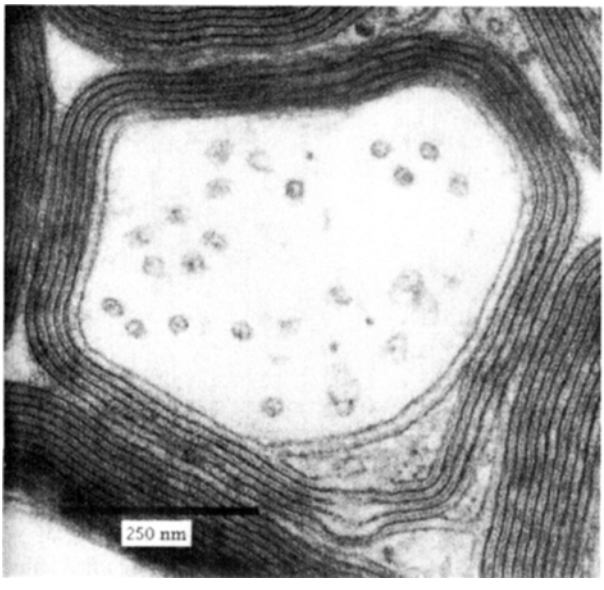

Fig. 6.14 Myelinated Axons Electron micrograph of a cross section through a portion of the optic fiber in an adult rat. The complete transverse section through a single myelinated axon is shown in close neighborhood to other axons. About four wrappings of myelin insulation are visible. The circular structures inside the axonal cytoplasm are transverse sections through microtubules. Reprinted by permission from Peters, Palay, and Webster (1976).

6. Pharmacological blockage of potassium channels has no effect on the shape of the action potential in the rabbit fibers (Ritchie, Rang, and Pellegrino, 1981).

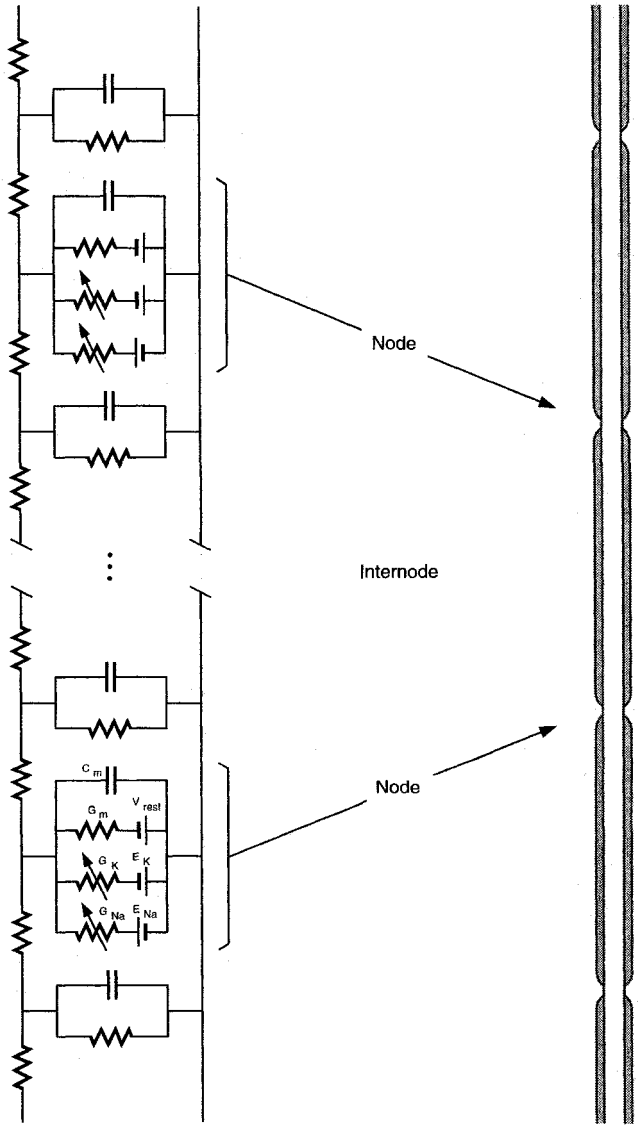

Fig. 6.15 Electrical Circuit for a Myelinated Axon Geometrical and electrical layout of the myelinated axon from the frog sciatic nerve (Frankenhaeuser and Huxley, 1964; Rogart and Ritchie, 1977). The diameter of the axon and its myelin sheath is 15 μm, the diameter of the axon itself 10.5 μm, the difference being made up by 250 wrappings of myelin. The myelin is interrupted every 1.38 mm by a *node of Ranvier* that is 2.5 μm wide. The total distributed capacitance for the internode (2.2 pF) is only slightly larger than the capacitance of the much smaller node (1.6 pF). The same is also true of the distributed resistance. At each node, the spike is reamplified by a fast sodium current and is repolarized by a potassium current. Little or no potassium current is found at the nodes of Ranvier in mammalian myelinated axons. There, repolarization is accomplished by rapid sodium inactivation in conjunction with a large effective "leak" current.

1995). Potassium channels are present under the myelin sheet along the internodal section, although their functional role is unclear (Waxman and Ritchie, 1985).

The function of the numerous tightly drawn layers of myelin around the internodal segments is to reduce the huge capacitive load imposed by this very large cable segment, as well as to reduce the amount of longitudinal current that leaks out across the membrane. The effective membrane capacitance of the entire myelin sheath, which in the case of the frog axon illustrated in Fig. 6.15, is made up of 250 myelin layers, is $C_m/250$, with C_m the specific capacitance of one layer of myelin (similar to that of the axonal membrane), while the effective resistance is 250 times higher than the R_m of one layer of myelin. Even though the length of the interaxial node is typically 1000 times larger than the node, its total capacitance has the same order of magnitude (Fig. 6.15). This allows the action potential to spread rapidly from one node to the next, "jumping" across the intervening internodal areas and reducing metabolic cost (since less energy must be expended to restore the sodium concentration gradient following action potential generation). There is a safety factor built into the system, since blocking one node via a local anesthetic agent does not prevent blockage of the impulse across the node (Tasaki, 1953). Detailed computer simulations of the appropriately modified Hodgkin–Huxely equations (based on the circuit shown in Fig. 6.15) have confirmed all of this (Frankenhaeuser and Huxley, 1964; Rogart and Ritchie, 1977).

Single axons can extend over 1 m or more,[7] making conduction velocity of the electrical impulses something that evolution must have tried to maximize at all cost. Measurements (Huxley and Stämpfli, 1949) and computations indicate that the time it takes for the currents at one node to charge up the membrane potential at the next node is limited by the time it takes to charge up the intervening internodal membrane. This is determined by the time constant of the membrane τ, which is independent of the geometry of the axon. In this time the spike will have moved across the internodal distance, making the propagation velocity proportional to this distance divided by τ. Since anatomically the internodal distance is linearly related to the diameter of the axon, the velocity of spike propagation will be proportional to the fiber diameter,

$$u \propto d \tag{6.29}$$

rather than the square-root dependency found for unmyelinated fibers (Eq. 6.27). Rushton (1951) gave this argument a precise form using the principle of *dimensional scaling*. If, he argued, axons had the same specific membrane properties, then in order for points along two axons with different diameters to be in "corresponding states," certain scaling relationships must hold. In particular, space should increase in units of the internodal length and velocity should be roughly proportional to the fiber diameter (for more details, see Weiss, 1996). The latter is actually the case (Fig. 6.16). When comparing the fiber diameter against the propagation velocity for myelinated cat axons, a roughly linear relationship can be observed (Hursh, 1939; Rushton, 1951; Ritchie, 1982). With the exception of a 1.1-μm-thick unmyelinated mammalian fiber that propagates action potentials at 2.3 mm/msec (Gasser, 1950), spike velocity in very small fibers has, so far, been difficult to record.

The functional importance of myelinated fibers is clear. They provide a reliable and rapid means of communicating impulses at a much reduced cost compared to unmyelinated fibers (at the same conduction velocity, a myelinated fiber can be up to 50 times thinner than an

7. Think about the spinal nerve axons of an elephant or of the extinct Brontosaurus.

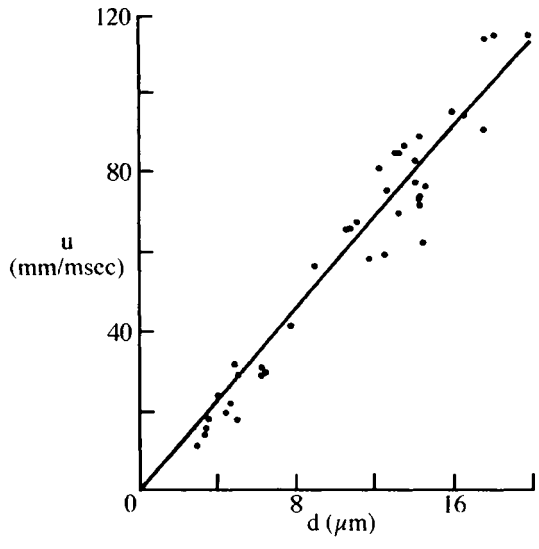

Fig. 6.16 Diameter and Propagation Velocity Relationship between (internal) diameter d of adult cat peripheral myelinated fibers and propagation velocity u of the action potential. The data are shown as dots (Hursh, 1939) and the least-square fit as a line. Peripheral myelinated fibers are bigger than 1 μm, while myelinated fibers in the central nervous system can be as thin as 0.2 μm, with an expected velocity in the 1-mm/msec range. Reprinted by permission from Ritchie (1982).

unmyelinated fiber). This large ($\times 2500$) factor in packing allows the brain to squeeze more than a million axons into a single nerve that supplies the brain with visual information. The primary cost of this insulation is the added developmental complexity and the possibility that demyelinating diseases, such as *multiple sclerosis*, can incapacitate the organism.

6.7 Branching Axons

The all-or-none nature of action potentials has lead to the idea that the axon serves mainly as a reliable transmission line, making a highly secure, one-way point-to-point connection among two processing devices. Furthermore, because of its high propagation velocity, the action potential is thought to arrive almost simultaneously to all of its output sites. Indeed, both properties have been used to infer that spikes propagating parallel fibers in the cerebellum serve to implement a very precise timing circuit (Braitenberg and Atwood, 1958; Braitenberg, 1967).

It will not come as a surprise that the axon-as-a-wire concept is not quite true and needs to be revised. Experimentally, it is known that trains of action potentials show failure at certain regions along the axon, most likely at the branch points. In other words, the train of spikes generated at the soma may have lost some of its members by the time it reaches the presynaptic terminals, with individual spikes "deleted" (Barron and Matthews, 1935; Tauc and Hughes, 1963; Chung, Raymond, and Lettvin, 1970; Parnas, 1972; Smith, 1983). For instance, conduction across a branching point in a lobster axon fails at frequencies above 30 Hz (Grossman, Parnas, and Spira, 1979a). This conduction block first appears in the thicker daughter branch and only later in the thinner branch, most likely due to a differential buildup of potassium ions (Grossman, Parnas, and Spira, 1979b). Physiological evidence indicates that such a switching mechanism might subserve a specific function in the case of the motor axon innervating the muscle used for opening the claw in the crayfish (Bittner, 1968). Depending on the firing frequencies, spikes are routed differentially into two branches of the axon going to separate muscle fibers.

These experimental studies have shown that action potentials may fail to invade the daughter branches of a bifurcating axon successfully. As the theoretical analysis by Goldstein and Rall (1974) pointed out, the single most important parameter upon which propagation past the bifurcation depends is its associated geometric ratio

$$\mathrm{GR} = \frac{d_{\mathrm{daughter},1}^{3/2} + d_{\mathrm{daughter},2}^{3/2}}{d_{\mathrm{parent}}^{3/2}} \tag{6.30}$$

where the d's are the fiber diameters and it is assumed that the specific membrane properties are constant in all three branches. This should remind us, of course, of the analysis of the branching passive cables (Secs. 3.1, 3.2, and Eq. 3.15) and, indeed, the reasoning is identical. GR equals the ratio of the input impedances if all cables are semi-infinite.

Goldstein and Rall's (1974) and subsequent analytical and modeling investigations (Khodorov and Timin, 1975; Parnas and Segev, 1979; Moore, Stockbridge, and Westerfield, 1983; Lüscher and Shiner, 1990a,b; Manor, Koch, and Segev, 1991) established the following principles. For GR = 1, *impedances match* perfectly and the spike propagates without any perturbation past the branch point (indeed, electrically speaking, for GR = 1 the branching configuration can be reduced to a single *equivalent cable*, albeit an active one; see Sec. 3.2). If GR < 1, the action potential behaves as if the axon tapers and it will slightly speed up. The far more common situation is GR > 1, that is, the combined electrical load of the daughters exceeds the load of the main branch. As long as GR is approximately < 10, propagation past the branch point is assured, although with some delay (that can be substantial for large values of GR). If GR> 10, propagation into both branches fails simultaneously, since the electrical load of the daughters has increased beyond the capacity of the electrical current from the parent branch to initiate a spike in the daughter branches. Parnas and Segev (1979) emphasize that for each constant geometric ratio, changes in the diameter ratio between the daughter branches never yields differential conduction into one of the daughters if the specific membrane properties are identical in both. This implies that the experimentally observed differential conduction (Bittner, 1968; Grossman, Parnas, and Spira, 1979a) must be due to other factors, such as a rundown in the ionic concentration across the membrane or saturation of the ionic pumps that are sensitive to the ratio of area to volume (and would thus be expected to occur earlier in larger fibers). Note that all of these modeling studies have assumed unmyelinated fibers and that axonal branch points appear to be devoid of myelin.

Up to 10–12 bifurcations (see the heavily branched axonal terminal arbor in Fig. 3.1M) can occur before the action potential reaches its presynaptic terminal where it initiates vesicular release. The delay at branch points with GR >1, in conjunction with other geometrical inhomogeneities, such as the short swellings at sites of synaptic terminals called *varicosities*, might add up to a considerable number, leading to a substantial broadening of spike arrival times at their postsynaptic targets.

The degree of temporal dispersion was simulated in the case of an axon from the somatosensory cortex of the cat (Manor, Koch, and Segev, 1991). Since it is almost entirely confined to cortical gray matter, it was taken to be unmyelinated (Fig. 6.17). In the absence of better data, Hodgkin–Huxley dynamics (at 20° C) were assumed. About 1000 boutons were added to the axon and the propagation time between spike initiation just beyond the cell body and these boutons is shown in the histogram of Fig. 6.17. The first peak (with a mean of 3.8 ± 0.5 msec) is contributed from terminals along the branches in cortical areas 3a and 3b (see the inset in Fig. 6.17A) and the more delayed one from those in area

4 (mean of 5.8± 0.4 msec). Of the total delay, about 22–33% is due to the branch points and geometrical inhomogeneities; the majority is simple propagation delay. Manor, Koch, and Segev (1991) conclude that temporal dispersion in the axonal tree will be minor, on the order of 0.5–1 msec.

Let us conclude with one observation. Computer simulations of branching axons by the author have shown that a strategically located inhibitory synapse of the shunting type onto one branch of the axon, following the on-the-path theorem (Sec. 5.1.3), can selectively veto an action potential from invading this branch while not affecting spike invasion into the second branch. This would allow for very fast synaptic switching or *routing* of information in an axonal tree (similar to a telephone network). While inhibitory synapses can be found directly at the axon initial segment (Kosaka, 1983; Soriano and Frotscher, 1989), no synapses, whether excitatory or inhibitory, have been observed on or around axonal branching points. It is anybody's guess why the nervous system did not avail itself of this opportunity to precisely (in space and time) filter or gate action potentials.

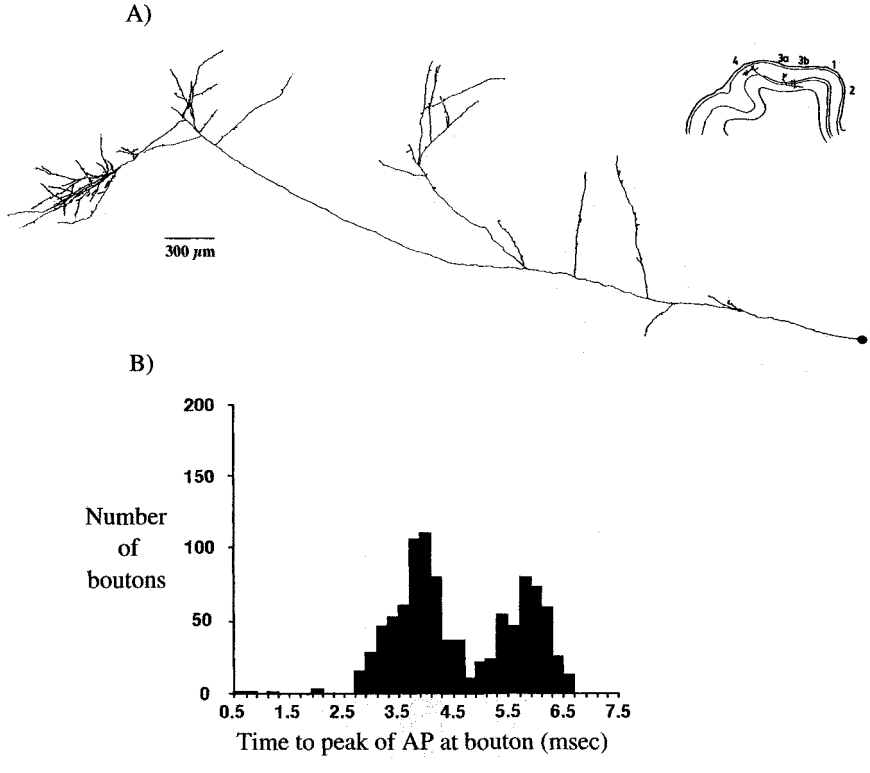

Fig. 6.17 PROPAGATION DELAYS ALONG A BRANCHING AXON Delays that action potentials incur as they propagate through a highly branching axonal tree **(A)**, simulated in the case of an HRP labeled axon originated in layer 5 of the somatosensory cortex of the adult cat (see inset). Reprinted by permission from Schwark and Jones (1989). **(B)** Histogram of the delay incurred between action potential initiation just beyond the cell body and the 977 terminals distributed in the terminal branches of the axon. The two humps correspond to locations in the proximal and distal parts of the axonal tree. Over the 3.5 mm of the tree, the total delay is 6.5 msec and temporal dispersion is minimal. Reprinted by permission from Manor, Koch, and Segev (1991).

6.8 Recapitulation

The Hodgkin–Huxley 1952 model of action potential generation and propagation is the single most successful quantitative model in neuroscience. At its heart is the depiction of the time- and voltage-dependent sodium and potassium conductances G_{Na} and G_K in terms of a number of gating particles. The state of G_{Na} is governed by three activation particles m and one inactivating particle h, while the fate of the potassium conductance is regulated by four activating particles n. The dynamics of these particles are governed by first-order differential equations with two voltage-dependent terms, the steady-state activation (or inactivation), and the time constant. The key feature of activating particles is that their amplitude increases with increasing depolarization, while the converse is true for inactivating particles. For rapid input to a patch of squid axonal membrane, spike initiation is exceeded whenever the net inward current becomes negative, that is, when a particular voltage threshold V_{th} is exceeded.

Inclusion of the cable term leads to a four-dimensional system of coupled, nonlinear differential equations with a wave solution that propagates at a constant velocity down the axon. This wave, the action potential, is due to the balance between dispersion and restoration caused by the voltage-dependent membrane. When injecting sustained currents into the axon, the equations predict two important aspects of the squid axon: the abrupt onset of sustained firing with a high spiking frequency and the very limited bandwidth of the firing frequency.

The Hodgkin–Huxley formalism represents the cornerstone of quantitative models of nerve cell excitability, and constitutes a remarkable testimony to the brilliance of these researchers. It should be remembered that their model was formulated at a time when the existence of ionic channels, the binary, microscopic, and stochastic elements underlying the continuous macroscopic, and deterministic ionic currents, was not known.

Wrapping axons in insulating material, such as the many layers of myelin observed in myelinated fibers that are found in all vertebrates, leads to a dramatic speedup over unmyelinated fibers. Conversely, at the same spike propagation speed, myelinated fibers can be up to 50 times thinner than unmyelinated fibers. In mammals, axons above 1 μm are usually myelinated, with speeds in the 5-mm/msec range, and rarely exceed 20 μm. When axons reach their target zone, they branch profusely, enabeling them to make thousands of contacts on postsynaptic processes. As trains of spikes attempt to propagate past these points, they can be slowed down, depending on the exact geometry of the junction. In the more extreme cases, individual spikes can fail to propagate past branch points.

We conclude that pulses can communicate along axons reliably, rapidly (at speeds between 1 and 100 mm/sec) and with little temporal dispersion. The main exception to this appears to be the propagation of trains of spikes past branching points. Here, due to a variety of phenomena, conduction block can occur, which will differentially route information into one of the daughter branches or prevent conduction alltogether.